Solid State Nuclear Magnetic Resonance 137 (2025) 102004

Contents lists available at ScienceDirect

Solid State Nuclear Magnetic Resonance

journal homepage: www.elsevier.com/locate/ssnmr

Extending ^{17}O transverse relaxation measurement to satellite transitions as a direct probe of molecular dynamics in solids

Yizhe Dai [a], Ivan Hung [b], Zhehong Gan [b], Gang Wu [a,*]

[a] Department of Chemistry, Queen's University, 90 Bader Lane, Kingston, Ontario, Canada, K7L 3N6
[b] National High Magnetic Field Laboratory, 1800 East Paul Dirac Drive, Tallahassee, FL, 32310, USA

ARTICLE INFO

Handling Editor: Prof D Bryce

ABSTRACT

We report utilization of transverse relaxation rate (R_2) of ^{17}O ($I = 5/2$) satellite transitions (STs) as a probe of molecular dynamics in solids. A simple theoretical model using spectral density functions is proposed to describe the general R_2 behaviors of half-integer quadrupolar nuclei in solids in the presence of molecular motion (or chemical exchange). Experimental ^{17}O R_2 data recorded for both CT and ST from ^{17}O-labeled $NaNO_2$ over a large temperature range are used to verify the theoretical predictions. Our theoretical model is shown to be fully consistent with a full quantum mechanical treatment of the chemical exchange problem involving half-integer quadrupolar nuclei in solids by numerically solving the Liouville-von Neumann equation. The new ^{17}O ST R_2 method was also applied to study the carboxylate flipping motion in two [^{17}O]carboxylic acid-pyridine adducts in the solid state. The advantages of the ST R_2 approach are discussed. This ST R_2 approach adds a new dimension to the currently available CT-based solid-state NMR techniques for probing molecular motion in solids.

1. Introduction

We have recently seen strong interests in using solid-state ^{17}O NMR to probe molecular dynamics in both organic solids and solid materials [1–23]. This wave of recent studies on molecular motion can be seen as a part of continuing efforts in expanding solid-state ^{17}O NMR spectroscopy into areas of organic/biological molecules and bio-materials [24–33]. In fact, solid-state ^{17}O NMR was already proven useful for studying molecular motion in some earlier studies of solid materials [34–38]. So far, probing molecular motion in solids by ^{17}O NMR methods (or by solid-state NMR for half-integer quadrupolar nuclei in general) has largely relied on detection of the central transition (CT, $m = +1/2 \leftrightarrow m = -1/2$) because this particular single-quantum transition is free of line broadening from the first-order quadrupole interaction, $Q^{(1)}$ [39]. With the aid of magic-angle spinning (MAS) and in some cases MQMAS [40], reasonably high spectral resolution can be achieved for ^{17}O at moderate magnetic fields, which can be further improved with the availability of ultrahigh magnetic fields [41].

The CT-based ^{17}O NMR techniques for studying molecular motion include (1) 1D CT line shape analysis under for static and MAS powder samples, (2) relaxation time measurements (T_1, T_2, $T_{1\rho}$) for static powder samples, (3) 2D EXSY experiments (under both MAS and static conditions), and (4) stimulated-echo signal analysis for static powder samples. However, in some cases, due to the presence of multiple sites and a combination of second-order quadrupole and anisotropic magnetic shielding interactions, the observed CT ^{17}O line shapes are not well defined, making it challenging to obtain precise dynamic information. In other cases, a particular technique may be useful only under certain conditions. For example, $T_{1\rho}$ measurement is limited only to static samples because MAS can cause further complication for spin-locking of half-integer quadrupolar nuclei [42]. In addition, a proper analysis of the experimental data often requires that all the ^{17}O NMR tensor parameters be known, a condition that may be difficult to meet beyond well-studied model compounds. In the literature, there are also examples where a combined experimental NMR/computational approach was employed in studying molecular motion in the solid state [16,43,44].

In parallel to the CT-based techniques for studying quadrupolar nuclei, there are also a suite of well-established solid-state NMR techniques that are based on detection of satellite transitions (ST, for example, $m = 1/2 \leftrightarrow m = 3/2$ or $m = -1/2 \leftrightarrow m = -3/2$). These ST-based techniques include SATRAS [45–47], STMAS [48,49], START-MAS [50], DQ-ST [51], ST-PROSPR [52], etc. Because it is generally

This article is part of a special issue entitled: Advancements in SSNMR published in Solid State Nuclear Magnetic Resonance.

* Corresponding author.
E-mail address: wugang@queensu.ca (G. Wu).

https://doi.org/10.1016/j.ssnmr.2025.102004
Received 10 March 2025; Received in revised form 27 March 2025; Accepted 14 April 2025
Available online 15 April 2025

more difficult to detect STs than CTs, the ST-based methods are not as widely employed as the CT-based methods. However, several workers did point out that STs can also be sensitive to molecular motion in solids on a time scale different from that of CT in solids [35,53–56]. In this work, we use ^{17}O NMR to demonstrate that transverse relaxation of STs can be used to study molecular motion in solids. We develop a new theoretical model to describe the intrinsic quadrupole transverse relaxation times for CT and STs and the influence of molecular motion on their transverse relaxations. This theoretical model was verified experimentally with extensive ^{17}O transverse relaxation data from both CT and ST recorded for a model compound, ^{17}O-labeled $NaNO_2$. Our theoretical model was shown to be consistent with the numerical solutions of the Liouville-von Neumann equation in the Liouville space. We further applied this ST transverse relaxation approach to study the carboxylate flipping motion in two ^{17}O-labeled carboxylic acid-pyridine adducts containing strong OHN hydrogen bonds.

2. Theory

The impact of molecular motion on solid-state NMR spectra of half-integer quadrupolar nuclei has been the focus of several studies in the literature [57–62]. All these previous studies, while employing various theoretical treatments of the quadrupole interaction, were primarily interested in changes of NMR line shapes in the presence of molecular motion. Their theoretical predictions were based exclusively on extensive numerical simulations. In this work, our goal is to develop a simple theoretical model from which dynamic information can be readily extracted from experimental transverse relaxation data collected for both CT and STs without the need of knowing a complete set of NMR tensors involved.

2.1. A simple theoretical model

In general, the transverse relaxation rate for a single-quantum transition from (I, m) state to (I, (m −1)) state can be written as [63]:

$$R_2 = (R_2)_{adiab} + \frac{1}{2}\left(\frac{1}{\tau_m} + \frac{1}{\tau_{m-1}}\right) \tag{1}$$

where $(R_2)_{adiab}$ is known as the adiabatic width and the second term is the so-called lifetime broadening (τ_m and τ_{m-1} are the lifetimes of the initial and final states). The adiabatic width is caused by any modulation of the transition frequency $\omega_{m,m-1}$ by external perturbation, whereas the lifetime broadening is related to the spin-lattice (longitudinal) T_1-like process.

Now let us first evaluate the lifetime broadening contribution for a half-integer quadrupolar nucleus in the presence of a strong magnetic field. In the discussion that follows, we use ^{17}O ($I = 5/2$) as an example, although the theoretical treatment is applicable to any I. The lifetime for the state with (I, m) is defined as τ_m where $m = \pm 1/2, \pm 3/2, \pm 5/2$ for $I = 5/2$. If the first-order quadrupole interaction, $Q^{(1)}$, is the main relaxation mechanism as a result of molecular motion in solids, it can be readily shown that the inverse lifetime ($1/\ \tau_m$) can be written as [63–65]:

$$\left(\frac{1}{\tau_{\pm 1/2}}\right) = K\left(\frac{16}{25}J_1 + \frac{56}{25}J_2\right) \tag{2}$$

$$\left(\frac{1}{\tau_{\pm 3/2}}\right) = K\left(\frac{56}{25}J_1 + \frac{36}{25}J_2\right) \tag{3}$$

$$\left(\frac{1}{\tau_{\pm 5/2}}\right) = K\left(\frac{40}{25}J_1 + \frac{20}{25}J_2\right) \tag{4}$$

where J_1 and J_2 are the standard spectral density functions. In general, for molecular motion with a correlation time τ_c, the standard spectral density functions are defined as:

$$J_n(n\omega_0) = \frac{\tau_c}{1 + (n\omega_0\tau_c)^2} \tag{5}$$

where n = 0, 1, and 2. The common factor K in eqs. (2)–(4) has the following expression [65]:

$$K = \frac{3}{160}\langle\omega_Q^2\rangle \tag{6}$$

where $\langle\omega_Q^2\rangle$ refers to the averaged value of the square of the nuclear quadrupole coupling constant ($\omega_Q = 2\pi C_Q$) over discrete molecular jumps in solids.

By combining the results from eqs. (2)–(6) into eq. (1), we can obtain the lifetime broadening contributions for the central transition (CT, $m = +1/2 \leftrightarrow m = -1/2$), the first pair satellite transitions (ST1, $m = +3/2 \leftrightarrow m = +1/2$ or $m = -1/2 \leftrightarrow m = -3/2$), and the second pair satellite transitions (ST2, $m = +5/2 \leftrightarrow m = +3/2$ or $m = -3/2 \leftrightarrow m = -5/2$) as:

$$CT : K\left(\frac{16}{25}J_1 + \frac{56}{25}J_2\right) \tag{7}$$

$$ST1 : K\left(\frac{36}{25}J_1 + \frac{46}{25}J_2\right) \tag{8}$$

$$ST2 : K\left(\frac{48}{25}J_1 + \frac{28}{25}J_2\right) \tag{9}$$

Now we turn our attention to the adiabatic width. In isotropic liquids, the adiabatic width in NMR of half-integer quadrupolar nuclei was extensively discussed in the literature especially in the slow motion regime [26]. In a rigid solid, if there is no substantial molecular motion, the adiabatic width should vanish. However, in the presence of molecular motion in solids such as 2-fold flips or C_3 jumps, the molecular motion/jumps will cause a fluctuation of the transition frequency $\omega_{m,m-1}$ because this frequency depends on the crystallite orientation. This modulation will give rise to a non-zero adiabatic width. As an example, let us consider a classic two-site chemical exchange problem with the frequency difference between the two sites being $\Delta\omega_{m,m-1}(t)$. For the CT, $\Delta\omega_{1/2,-1/2}$ is determined by the second-order quadrupole frequency shift, $\Delta\omega_{Q2}$ is on the order of ω_Q^2/ω_0 where ω_Q is the first-order quadrupole frequency). Under such a circumstance, the adiabatic width can be written as:

$$\langle\Delta\omega_{Q2}^2\rangle J_1(\Delta\omega_{Q2}) = \langle\Delta\omega_{Q2}^2\rangle \frac{\tau_c}{1 + (\Delta\omega_{Q2}\tau_c)^2} \tag{10}$$

where $\langle\omega_{Q2}^2\rangle$ is the averaged value of the square of the second-order quadrupole frequency shift over molecular motion/jumps in solids. As a result, combining eqs. (7) and (10) into (1) gives us the total transverse relaxation for the CT as

$$(R_2)^{CT} = \frac{3}{160}\langle\omega_Q^2\rangle\left[\frac{16}{25}J_1(\omega_0) + \frac{56}{25}J_2(2\omega_0)\right] + \langle\Delta\omega_{Q2}^2\rangle J_1(\Delta\omega_{Q2}) \tag{11}$$

The same argument applies to ST1, except that the ST1 transition frequency contains both the first- and second-order quadrupole frequency shifts. For brevity, we denote the ST1 frequency difference between the two sites as $\Delta\omega_{ST1}$. Then we can write the total transverse relaxation for ST1 as

$$(R_2)^{ST1} = \frac{3}{160}\langle\omega_Q^2\rangle\left[\frac{36}{25}J_1(\omega_0) + \frac{46}{25}J_2(2\omega_0)\right] + \langle\Delta\omega_{ST1}^2\rangle J_1(\Delta\omega_{ST1}) \tag{12}$$

and, similarly, for ST2 as

$$(R_2)^{ST2} = \frac{3}{160}\langle\omega_Q^2\rangle\left[\frac{48}{25}J_1(\omega_0) + \frac{28}{25}J_2(2\omega_0)\right] + \langle\Delta\omega_{ST2}^2\rangle J_1(\Delta\omega_{ST2}) \tag{13}$$

Now with eqs. (11)–(13), we are able to predict how R_2 data would behave for both CT and STs. Fig. 1a shows typical R_2 curves as a function

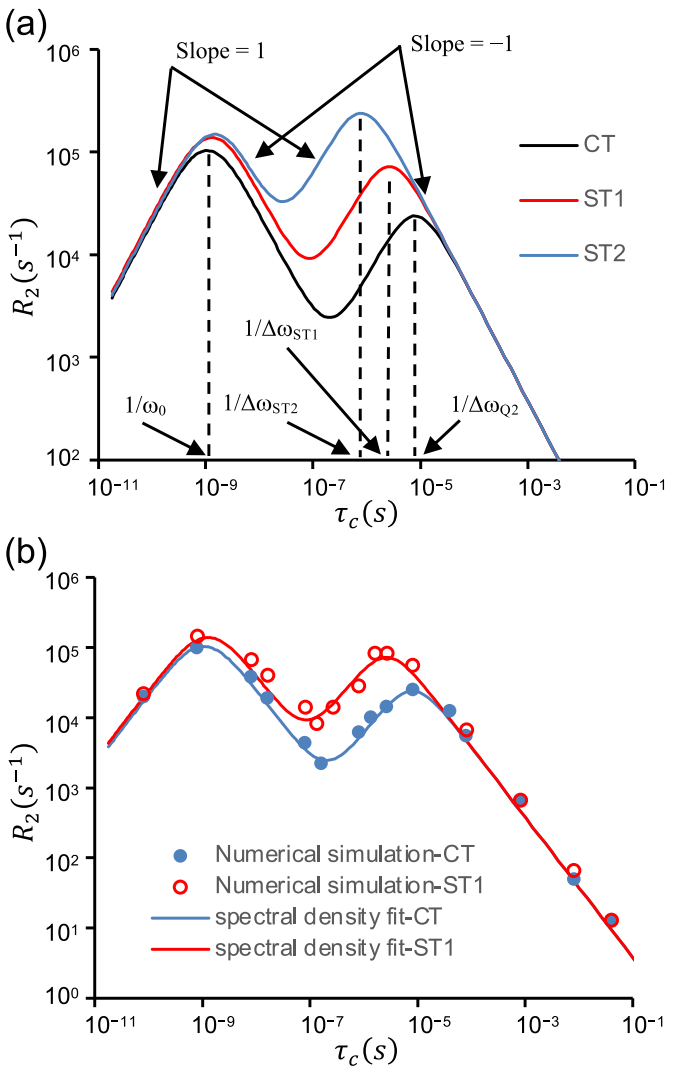

Fig. 1. (A) Illustration of transverse relaxation R_2 curves as a function of molecular correlation time (τ_c) for CT, ST1, and ST2 for $I = 5/2$. The parameters used to produce these curves are: $\omega_0 = 2\pi \times 95 \times 10^6$ (rad/s), $\omega_Q = 2\pi \times 10 \times 10^6$ (rad/s), $\Delta\omega_{Q2} = 2\pi \times 20 \times 10^3$ (rad/s), $\Delta\omega_{ST1} = 2\pi \times 60 \times 10^3$ (rad/s), $\Delta\omega_{ST2} = 2\pi \times 200 \times 10^3$ (rad/s). (b) Comparison between numerical simulations and spectral density fits with eqs. (11)–(13) where $\tau_c = (2k_{ex})^{-1}$.

of molecular correlation time, τ_c. Each of the R_2 curves clearly shows two distinct transitions, as first pointed out by Hung et al. [12] for changes in the CT line shape due to chemical exchange. As seen in Fig. 1a, the CT R_2 undergoes the first transition when the molecular motion is comparable with the second-order quadrupole shift, $\Delta\omega_{Q2}$, i.e., when $\tau_c = (\Delta\omega_{Q2})^{-1}$. As expected, the first transition for the ST1 occurs at a shorter τ_c than the transition for the CT. This is because the relevant frequency difference, $\Delta\omega_{ST1}$, depends on both the first- and second-order quadrupole interactions and is considerably larger than $\Delta\omega_{Q2}$. Thus, the first transition for the ST1 occurs at $\tau_c = (\Delta\omega_{ST1})^{-1} > (\Delta\omega_{Q2})^{-1}$. Similarly, the first transition for the ST2 lags further behind occurring at $\tau_c = (\Delta\omega_{ST2})^{-1}$, because $\Delta\omega_{ST2} > \Delta\omega_{ST1} > \Delta\omega_{Q2}$. After the first transitions, as seen in Fig. 1a, the second transition occurs simultaneously for CT, ST1, and ST2 all at $\tau_c = (\omega_0)^{-1}$. Around the second transition, transverse relaxations for CT, ST1, and ST2 are exclusively determined by lifetime broadening.

The most important feature in the R_2 curves shown in Fig. 1a is the fact that all three R_2 curves share exactly the same slope in the slow-motion region (a slope of −1 on a double logarithm scale). It can be readily shown that this slope yields the information about the activation energy for the molecular jumps once a kinetic model is introduced (*vide infra*). As is clear from Fig. 1a, the benefit of measuring R_2 for all CT, ST1 and ST2 transitions (if possible) is to extend the temperature range for the region with a slope of −1 so that activation energy can be measured with the greatest accuracy. It is also important to note that several other regions also display slopes of −1 or 1. One region is between the two maxima for each R_2 curve and the other is at the fast motion regime. However, one can anticipate some difficulties in utilizing these two regions in practice. For all three transitions, the region between the two maxima spans a rather narrow temperature range making it difficult to allow many data points to be collected. The fast motion region is often prohibited to be accessed either by the practical limitation of high temperatures or sample melting.

To confirm the validity of the spectral density function approach based on eqs. (11)–(13), we employed a full quantum mechanical treatment of the chemical exchange problem involving quadrupolar nuclei in the solid state. As described in a previous study [12], the evolution of a spin system can be generally described in the Liouville space by

$$\frac{d}{dt}\sigma = \hat{\hat{\mathscr{L}}}\sigma \tag{14}$$

where σ is the density operator and the Liouvillian $\hat{\hat{\mathscr{L}}}$ includes both the Hamiltonian and relaxation superoperators. For a two-site chemical exchange problem, σ and $\hat{\hat{\mathscr{L}}}$ can be expressed as

$$\sigma = \begin{pmatrix} \sigma_A \\ \sigma_B \end{pmatrix}, \quad \hat{\hat{\mathscr{L}}} = \begin{pmatrix} \hat{\hat{\mathscr{L}}}_A - k_{ex}\mathbb{I} & k_{ex}\mathbb{I} \\ k_{ex}\mathbb{I} & \hat{\hat{\mathscr{L}}}_B - k_{ex}\mathbb{I} \end{pmatrix} \tag{15}$$

where k_{ex} represents the exchanging rate between sites *A* and *B*. All terms of the quadrupolar interaction including those with off-diagonal elements along with the Zeeman Hamiltonian are included in $\hat{\hat{\mathscr{L}}}_A$ and $\hat{\hat{\mathscr{L}}}_B$. The perturbation from those off-diagonal elements will be automatically taken into account for the high-order quadrupolar shift in the process of solving the equation by finding the eigenvalues of $\hat{\hat{\mathscr{L}}}$. The imaginary part of the eigenvalues gives rise to oscillations while the real part corresponds to decay of the coherences. For the transverse relaxation calculation, because the oscillatory part is refocused by the spin-echo, only the real part is kept for signal decay of single-quantum coherences (both CT and STs). The selection between CT and STs is controlled by the frequency range set for powder averaging.

Here we used this full quantum mechanical approach to compute ^{17}O R_2 values for both CT and ST1 for a powder sample of $NaNO_2$ where the 180°-flipping motion of the nitrite anion was well characterized in the literature [10]. As seen from Fig. 1b, an excellent agreement was found between the numerical simulations and the spectral density fittings based on eqs. (11)–(13). In the numerical simulations, all ^{17}O NMR tensor parameters reported for solid $NaNO_2$ by Dai et al. [10] were used. It is important to point out that, in the positive slope regions ($10^{-7} < \tau_c < 10^{-5}$ s in Fig. 1b), the numerical simulations suggest that both CT and ST1 display bi-exponential or multi-exponential decays. However, because the fast decaying component for ST1 has exceedingly short T_2 values (ca. 1 μs), we chose the slow decaying component in the plot. In contrast, the fast decaying component of CT has T_2 values of greater than 50 μs, which can be readily detected experimentally (*vide infra*). Another possible contribution to the non-exponential decays seen in the numerical simulations is a small mixing of the ST1 signal into the CT (or mixing of the ST2 into ST1). Although this kind of signal mixing is expected to be rather small on the basis of their vastly different spectral widths, they may become visible when the mixed signals have very different T_2 values. In practice, one can minimize the possible mixing of ST2 into ST1 by setting the transmitter close to the "horn" position of the ST1 powder pattern, which occurs at $3C_Q(1-\eta_Q)/40$ from the isotropic

chemical shift position for $I = 5/2$ (ignoring the second-order quadrupole shift in ST1). In addition, the non-exponential behavior also introduces uncertainties for the T_2 values used in the theoretical curve shown in Fig. 1b, which appears to exhibit small variations (or "noise") in the critical region ($10^{-7} < \tau_c < 10^{-5}$ s). Recently, Vugmeyster et al. [22] applied a similar Liouvillian formalism to treat the nitrate C_3-jumps in solid $NaNO_3$. Our results shown in Fig. 1b are in agreement with their ^{17}O CT R_2 and $R_{1\rho}$ curves.

3. Experimental section

The preparation of ^{17}O-labeled $NaNO_2$ was reported previously [10]. Preparation of the adduct of 3,5-dinitro-[$^{17}O_2$]benzoic acid and 3,5-dimethylpyridine was carried out in the following way. 3,5-dinitrobenzoic acid (3,5-DNB, 200 mg, 0.943 mmol) was loaded to a 5 mL pressure tube, to which 140 μL ^{17}O-enriched H_2O (40 % ^{17}O atom, purchased from CortecNet) was added, followed by addition of 1.5 mL 4 M HCl in dioxane. The mixture was then heated in an oil bath at 110 °C for 12 h. Upon cooling of the solution to room temperature, most of the solvent was removed with a rotary evaporator until a very viscous liquid was obtained. The viscous liquid was then dissolved in 5 mL acetonitrile and transferred to a 25 mL round bottom flask. 3,5-dimethylpyridine (DMP) (110 mg, 1.03 mmol), which is an oily liquid at room temperature, was added to the flask. The mixture was stirred for 1 h. Evaporating of the acetonitrile with a gentle flow of N_2 gas led to formation of white solids. The while solids were filtered out and dried under vacuum overnight. 210 mg [$^{17}O_2$]-3,5-DNB-DMP adduct (0.66 mmol) were obtained. The ^{17}O enrichment level in the final product was estimated to be 25 % from solution-state ^{17}O NMR experiment. The pyridinium 2,4-dinitro-[$^{17}O_2$]benzoate adduct was prepared in a similar fashion as described above, except that 200 mg 2,4-dinitrobenzoic acid (2,4-DNB) were used and that 100 mg pyridine were added to 2,4-dinitro-[$^{17}O_2$] benzoic acid. The reaction yielded 150 mg pyridinium 2,4-dinitro-[$^{17}O_2$]benzoate as a white solid. The ^{17}O-enrichment level in the compound was estimated to be 26 % from solution-state ^{17}O NMR experiment.

^{17}O transverse relaxation times (T_2) were measured using the spin-echo pulse sequence on Bruker Avance-500 (11.7 T) and NEO-700 (16.4 T) NMR spectrometers at different temperatures. Typically, the echo delay was varied between 10 and 200 μs. The T_2 values were determined from the relative echo intensities in time domain. The CT and ST measurements were differentiated by setting the transmitter frequency offset to 500 and 7000 ppm, respectively. Powder sample was packed into a glass tube (5 mm o. d.). The ^{17}O chemical shifts were referenced to the signal of liquid H_2O at 0 ppm.

4. Results and discussion

4.1. ^{17}O-labeled $NaNO_2$ as a test case

To test the theoretical predictions described in Section 2.1, we recorded ^{17}O R_2 data for both CT and ST1 for a model compound, ^{17}O-labeled $NaNO_2$. In the crystal lattice of $NaNO_2$, the $[NO_2]^-$ anion is known to undergo 2-fold flipping motion and its dynamics was extensively studied [10]. Fig. 2 shows the ^{17}O CT and ST1 NMR signals from a powder sample of ^{17}O-labeled $NaNO_2$ at 16.4 T. To measure R_2 for CT and ST1, the transmitter was set to 500 and 7000 ppm, respectively. The CT signal displays a characteristic line shape due to a combination of

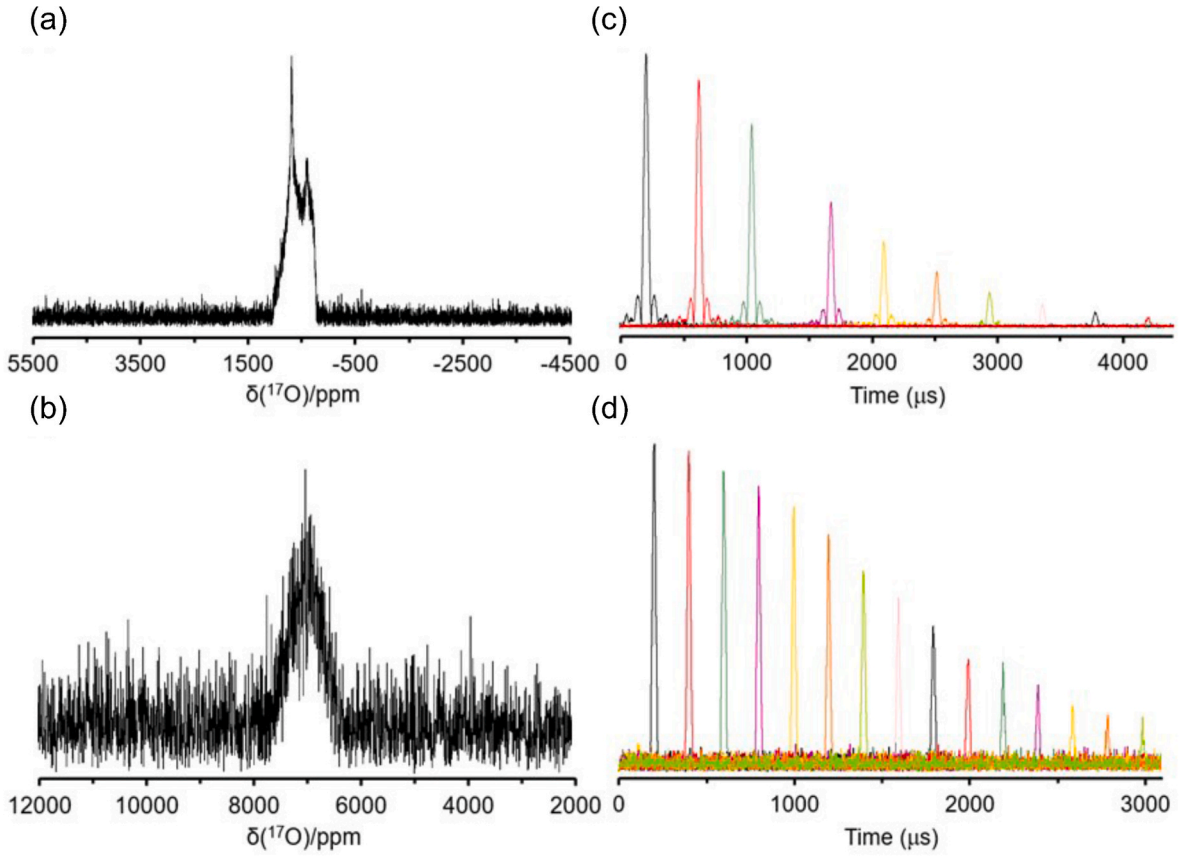

Fig. 2. Experimental ^{17}O NMR signals for ^{17}O-labeled $NaNO_2$ at 224 K from (a) CT (transmitter set at 500 ppm; echo delay 100 μs; 2500 transients; recycle delay 0.1 s) and (b) ST1 (transmitter set at 7000 ppm; echo delay 100 μs; 40000 transients; recycle delay 0.1 s). In (a) and (b), because a whole echo was collected in each case, the signal was shown in the magnitude mode. (c) and (d) are overlays of the spin-echoes collected with different echo delays for CT and ST1, respectively. In (c) and (d), the original FIDs without any manipulation are shown to illustrate the true signal-to-noise ratio.

second-order quadrupole interaction and chemical shift anisotropy. But the ST1 signal is just a featureless Gaussian-type line shape, because it represents only a small piece of a very wide ST1 powder line shape. As also seen from Fig. 2, the ST1 signal is considerably weaker than the CT. But in the time domain, both CT and ST1 echoes display excellent signal-to-noise ratios. The T_2 values were determined for both CT and ST1 from the time-domain decays collected with the spin-echo sequence.

Fig. 3 displays all the experimental R_2 data for CT and ST1 and fitting with our theoretical model using eqs. (11)–(13). It should be pointed out that, at a few temperatures around 284 K (1000/T ≈ 3.5 in Fig. 3), we observed bi-exponential characteristics in the T_2 decays for CT. In each of these cases, we displayed the shorter T_2 value in Fig. 3. In contrast, all ST1 T_2 decays are good exponential decays at all temperatures studied. We will further discuss this issue in the next section. To fit the data shown in Fig. 3 with our theoretical model, we assume the following Arrhenius equation to describe the temperature dependence of τ_c (or k_{ex}):

$$\tau_c = (2k_{ex})^{-1} = \tau_0 \, exp\left(\frac{E_a}{RT}\right) \tag{16}$$

where E_a is the activation energy for the molecular jumps, τ_0 is the pre-exponential factor, and R is the gas constant.

It is well known that, while modulation of electric-field-gradient (EFG) due to large amplitude molecular motions such as the 180° flipping of the nitrite anion in Na_2NO_2 is the predominant relaxation mechanism for quadrupolar nuclei in solids, vibrations of apparent rigid atomic lattice known as phonon will also be a relaxation mechanism. For completeness, one should also consider in this work the Raman two-phonon relaxation process (a fluctuation of the first-order quadrupole interaction, $Q^{(1)}$, at the nucleus under observation induced by lattice vibration. Thus, $(R_2)_{phonon}$ can be considered as the *intrinsic* transverse relaxation in the absence of any chemical exchange. The Raman two-phonon relaxation is known to exhibit a weak temperature dependence in the following fashion [66]:

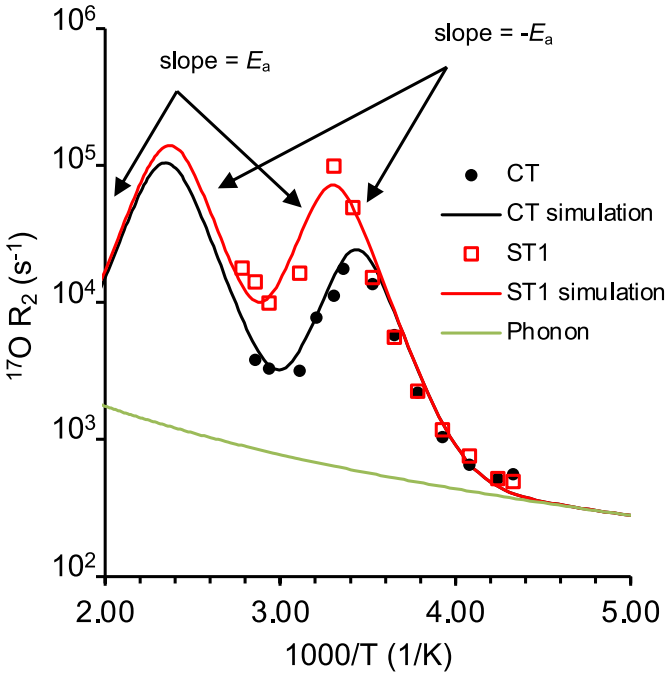

Fig. 3. Comparison between experimental ^{17}O R_2 data (data points) and fitting curves (solid lines) for CT and ST1 obtained for a static powder sample of ^{17}O-labeled $NaNO_2$ at 16.4 T. For the Raman two-phonon process, $C = 7.0 \times 10^3$ Hz K^2. Other fitting parameters used are: $\omega_0 = 2\pi \times 95 \times 10^6$ (rad/s), $\omega_Q = 2\pi \times 10 \times 10^6$ (rad/s), $\Delta\omega_{Q2} = 2\pi \times 20 \times 10^3$ (rad/s), and $\Delta\omega_{ST1} = 2\pi \times 60 \times 10^3$ (rad/s).

$$(R_2)_{Phonon} = (R_1)_{Phonon} = CT^2 \tag{17}$$

where C is a constant related to the averaged amplitude of the $Q^{(1)}$ interaction in the system. In this work, C can be treated as a fitting parameter. In general, $(R_2)_{Phonon}$ is the smallest contribution among all other relaxation mechanisms for quadrupolar nuclei in solids. In some cases where abundant quadrupolar spins are involved, the homonuclear dipolar interaction may be another source of relaxation as part of the intrinsic transverse relaxation. However, in the present study of ^{17}O, we can safely ignore any homonuclear dipolar contribution.

As seen from Fig. 3, we were able to satisfactorily reproduce the experimental R_2 data for both CT and ST1 using our model, from which we determined that $E_a = 68 \pm 1$ kJ/mol and $\tau_0 = 0.5 \times 10^{-17}$ s. These values are in excellent agreement with those previously determined from the extensive ^{17}O line shape analysis for CT spectra of the same compound recorded at four magnetic fields, 68 ± 5 kJ/mol [10,67]. The benefit of the approach demonstrated here is that the fitting of the R_2 curves shown in Fig. 3 does not require any information about ^{17}O NMR tensors. As also seen in Fig. 3, the activation energy, E_a is directly reflected on the slopes of the curves. The most important portion of the curve is the slope in the slow-motion regime. In this region, both CT and ST1 data points should partially overlap. Again, the benefit of having ST1 data is that they span a larger temperature range than the CT data, which will make the determination of E_a more accurate. As a practical matter, one can start the measurement of R_2 for the CT while stepping up the sample temperature until R_2 for the CT reaches its maximal value. Then one switches to measure R_2 for the ST1 at even higher temperatures until the R_2 for ST1 reaches its own maximal value. It is also interesting to note that, in $NaNO_2$, the Raman two-phonon process becomes important at temperatures below 243 K (1000/T > 4.0 in Fig. 3).

It is important to mention that, in this work, we used exclusively the spin-echo sequence to obtain CT and ST R_2 data. Although we did use the QCPMG sequence to collect some T_2 data for both CT and ST at certain temperatures, we observed significant discrepancies between the two methods. In addition, the T_2 value also appears to depend on the interpulse delay used in the QCPMG sequence. Furthermore, in practice it was not possible to use the QCPMG method to measure some very short T_2 values for both CT and ST. Some other issues related to QCPMG were well documented in the literature [68]. For these reasons, we excluded the R_2 data collected by the QCPMG sequence. A detailed study on the difference in quadrupole relaxation T_2 data by the spin-echo and CPMG sequences will appear later.

4.2. *Discussion about bi-exponential T_2 decays*

During the T_2 measurements for CT, we noticed that, at some temperatures especially on the fast side of the Q2 transitions (the intermediate region showing a positive slope), the T_2 decays exhibit significant deviations from a single exponential decay. For ST1, we did not observe this over the temperature range studied. As mentioned earlier, the numerical simulations suggest that the ST1 can exhibit bi-exponential characteristics as well. However, because the fast decaying component of ST1 has very short T_2 values (ca. 1 μs), it cannot be detected experimentally. In comparison, the fast decaying component of CT has much longer T_2 values (>50 μs). The observed non-exponential T_2 decays are fundamentally linked to the T_2 anisotropy often observed in the CT powder spectra (i.e., in the frequency domain). For example, Hoffmann et al. [20] observed significant T_2 anisotropies in the ^{17}O CT from a powder sample of low-density amorphous ice at 128.9 K. More recently, Vugmeyster et al. [22] also reported observation of non-exponential T_2 decays in ^{17}O CT NMR for a powder sample of $NaNO_3$. To illustrate this phenomenon, Fig. 4 shows the T_2 decays for CT recorded at 243, 283, and 353 K. Clearly, the T_2 decays at 243 and 353 K are essentially exponential, but that at 283 K shows a prominent bi-exponential character. This phenomenon can be easily understood by considering the

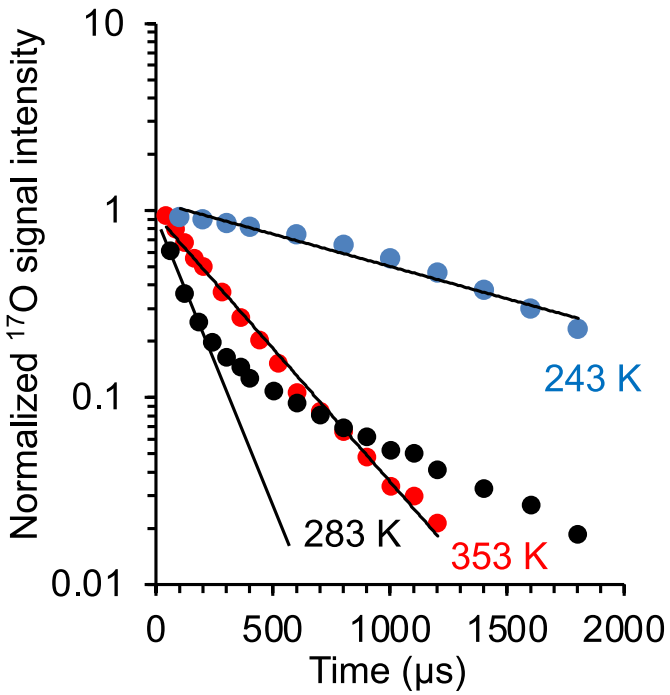

Fig. 4. Comparison of exponential and bi-exponential ^{17}O T_2 decays observed for the CT in ^{17}O-labeled $NaNO_2$ at 16.4 T.

dynamic effect on powder spectra. Let us first examine the exchange broadening at the CT. As is illustrated in Fig. 5, in the T_2 measurement for the CT, one often can excite the whole $Q^{(2)}$ powder pattern. The molecular reorientation due to motion causes two crystallites to undergo two-site chemical exchange, with the frequency difference between the two signals being on the order of $\Delta\omega_{Q2}$. When the motion is slow, all signals experience the same or very similar exchange broadening, which is proportional to k_{ex}. When the motion increases to become comparable to $\Delta\omega_{Q2}$ for some crystallites, these crystallites more significant broadening than others, thus giving rise to bi-exponential T_2 decays when all crystallites are observed together. When the motion continues to increase so that k_{ex} is now greater than $\Delta\omega_{Q2}$ for all crystallites, the exchange broadenings once again become similar for all crystallites. That is why the bi-exponential or non-exponential T_2 decays are observed only at the intermediate temperatures. The situation for the ST is quite different. As seen in Fig. 5, now the frequency difference between any pair of motion-related crystallites, $\Delta\omega_{ST1}$, is much larger than that for the CT. As a result, all crystallites would experience the same exchange broadening for a wide range of k_{ex}. Even in the fast motion region, all crystallites within the RF excitation profile would still have similar T_2 values.

4.3. *Carboxylate flipping in compounds containing OHN hydrogen bonds*

After having used the model compound $NaNO_2$ to demonstrate the ST R_2 approach, we apply this new method to study the carboxylate flipping motion in two molecular adducts: 3,5-dinitro-[$^{17}O_2$]benzoic acid-3,5-dimethylpyridine adduct (referred to as [^{17}O]-3,5-DNB-DMP in this work) and pyridinium 2,4-dinitro-[$^{17}O_2$]benzoate adduct (denoted as Py-[^{17}O]-2,4-DNB in this work). The reason for choosing these two

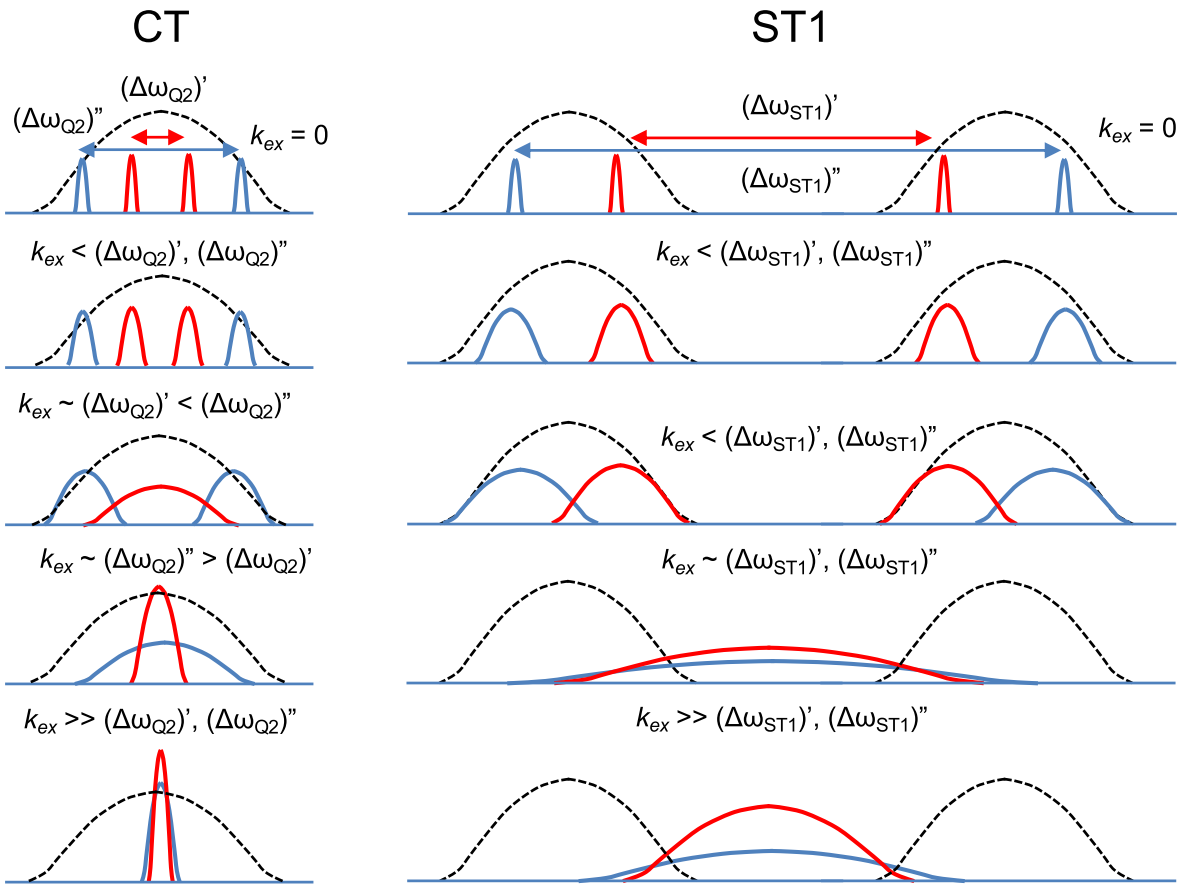

Fig. 5. Illustration of the dynamic effects on signals arising from different crystallites as the origin of the bi-exponential T_2 decays observed mostly for CT in the intermediate exchange regions. The dashed envelope indicates the excitation profile of the RF pulse.

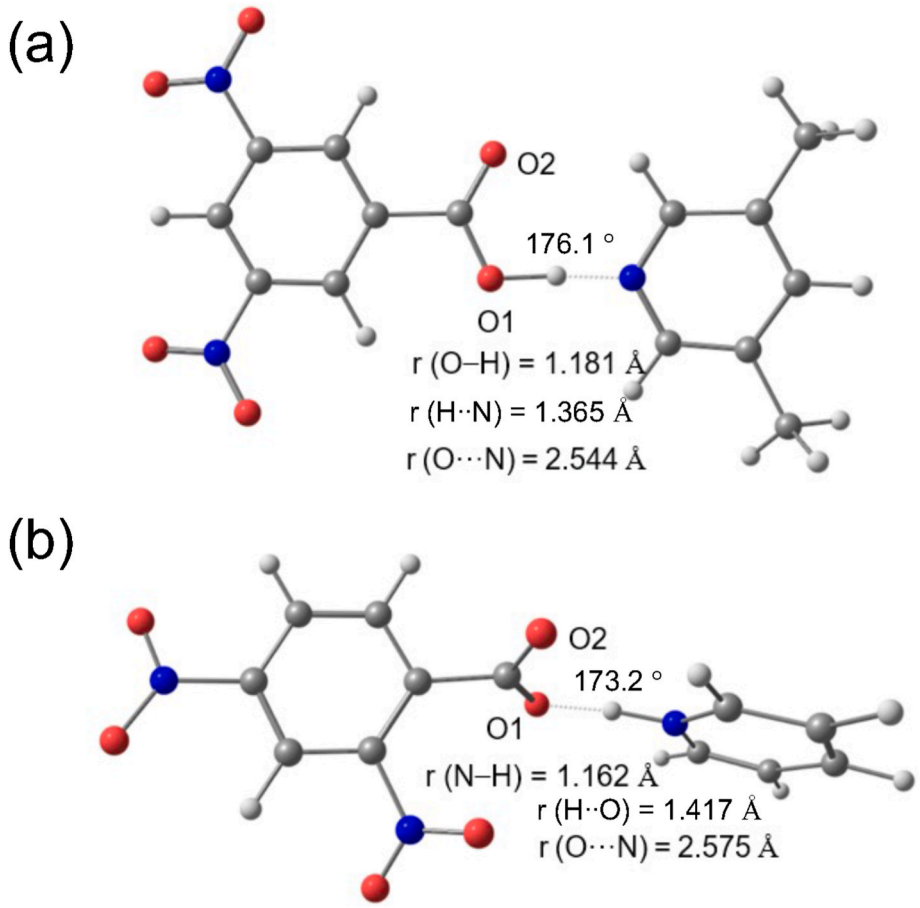

Fig. 6. Partial neutron diffraction crystal structures of (a) 3,5-DNB-DMP and (b) Py-2,4-DNB showing the two different types of OHN hydrogen bonds.

compounds is that they represent two extremes of the very strong OHN hydrogen bonds. As seen in Fig. 6, the neutron diffraction crystal structure of 3,5-DNB-DMP suggests that the central hydrogen atom is closer to the oxygen atom on the carboxylic acid group [69]. So the OHN hydrogen bond in this compound is considered to be of the O−H···N type with the O···N distance being 2.544 Å, which is among the shortest values reported in the literature. In comparison, the central hydrogen atom in Py-2,4-DNB is closer to the nitrogen atom of pyridine, making the hydrogen bond to be of the O···H−N type [70]. It is important to note that the O···N distance in Py-2,4-DNB is also rather short, 2.575 Å. Clearly, on the basis of the neutron diffraction structures, the hydrogen bonds in these two compounds are strong, but exhibit distinct structural features. As previously shown by Lu et al. [13] in the case of nicotinic acid, the carboxylate flipping motion in this kind of OHN hydrogen bonds is fundamentally linked to the hydrogen bond energetics.

To investigate whether the carboxylate flipping motion can reflect the different hydrogen bonding environments in 3,5-DNB-DMP and Py-2,4-DNB, we collected ^{17}O ST1 R_2 data for these two compounds. Fig. 7 shows the experimental results and theoretical fitting. Our analysis yielded the following results: for 3,5-DNB-DMP, $E_a = 58 \pm 2$ kJ/mol and $\tau_0 = 2.5 \times 10^{-16}$ s and for Py-2,4-DNB, $E_a = 40 \pm 2$ kJ/mol and $\tau_0 = 5.0 \times 10^{-13}$ s. As also seen in Fig. 7, significant Raman two-phonon contributions were observed in both cases. Interestingly, the static ^{17}O CT NMR spectra at either 11.7 T or 16.4 T of these two compounds (not shown) do not display enough detailed features which makes a proper line shape analysis rather challenging. Here we were able to obtain dynamic information from the ST R_2 approach without knowing the relevant ^{17}O NMR tensor parameters. Compared with the result of $E_a =$ 48 kJ/mol reported for nicotinic acid by Lu et al., [13] the corresponding values found for 3,5-DNB-DMP and Py-2,4-DNB are higher and lower, respectively. The discrepancy can be understood on the basis of the OHN hydrogen bonds formed in the two compounds. As mentioned earlier, the O−H···N hydrogen bond in 3,5-DNB-DMP is strong. In order for the carboxylate group to flip, the hydrogen atom must first migrate to the N end forming an intermediate like O···H−N. This hydrogen migration in 3,5-DNB-DMP costs extra energies. In the case of Py-2, 4-DNB, however, the hydrogen atom is already on the N end, i.e., the O···H−N hydrogen bond. Thus, flipping the carboxylate group is easier in Py-2,4-DNB than in 3,5-DNB-DMP.

5. Conclusions

We have demonstrated that ^{17}O ST R_2 data can be used to obtain dynamic information about molecular motion in solids. Our simple theoretical model using spectral density functions clearly shows the two transitions in the transverse relaxation as a response to molecular motion in the solid state. This physical model was shown to be consistent with the numerical simulations by solving the Liouville-von Neumann equation in the Liouville space for the chemical exchange problem involving quadrupolar nuclei. The ST-based approach has the advantage of having a larger "NMR frequency window" than does the CT. Of course, the disadvantage of the ST R_2 method is that the ST generally has weaker signal intensity than the CT. But it is important to point out that, because the ST relaxation measurement is carried out in the time domain, its sensitivity is in fact far superior than that often encountered when working with CT powder line shapes in the frequency domain. In practice, the most efficient way to obtain the activation energy of the motion is to combine CT R_2 and ST R_2 data in the slow-motion region. That is, one can start with the measurement of CT R_2 data until the CT reaches its first transition and then continue to collect ST1 R_2 data until

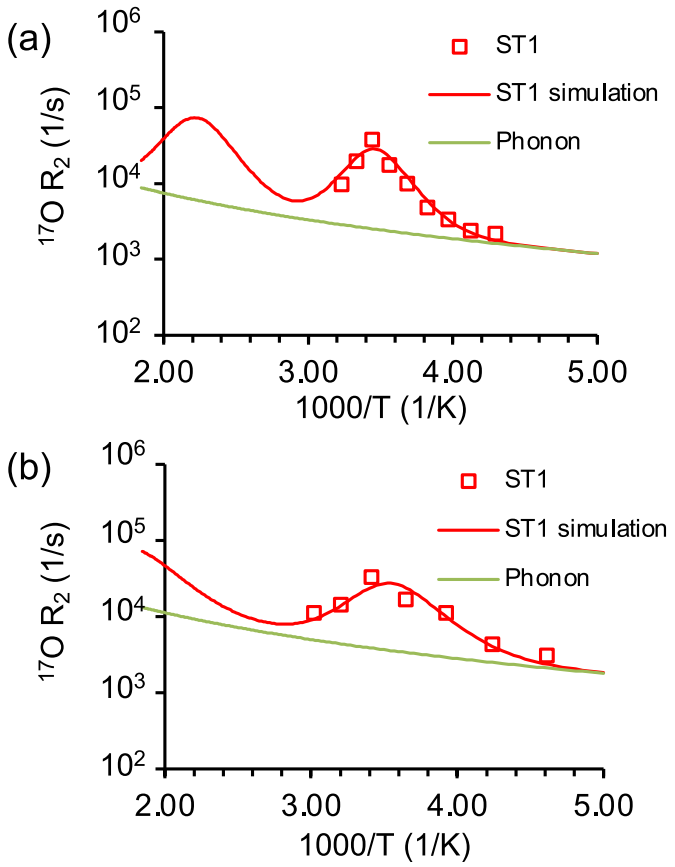

Fig. 7. Comparison between experimental ^{17}O R_2 data for ST1 (data points) and fitting curves (solid lines) obtained for static powder samples of (a) 3,5-DNB-DMP and (b) Py-2,4-DNB at 16.4 T. The green line indicates the contribution from the Raman two-phonon process. Other fitting parameters used are: (a): $\omega_0 = 2\pi \times 95 \times 10^6$ (rad/s), $\omega_Q = 2\pi \times 7 \times 10^6$, $\Delta\omega_{ST1} = 2\pi \times 22 \times 10^3$ (rad/s), $C = 3.0 \times 10^4$ Hz K^2; (b): $\omega_0 = 2\pi \times 95 \times 10^6$ (rad/s), $\omega_Q = 2\pi \times 7 \times 10^6$ (rad/s), $\Delta\omega_{ST1} = 2\pi \times 20 \times 10^3$ (rad/s), $C = 4.5 \times 10^4$ Hz K^2.

the ST1 also reaches its own first transition. This will ensure the largest temperature span accessible, from which the most accurate determination of activation energy can be achieved. Very often, one is limited by the shortest T_2 value that can be experimentally determined with the currently available technology (ca. a few μs). Finally, it should be emphasized that, while this study is concerned with solid-state ^{17}O NMR for static samples, the strategy demonstrated here is certainly applicable to all other half-integer quadrupolar nuclei under both static and MAS conditions.

Declaration of competing interest

The authors declare that they have no known competing financial interests or personal relationships that could have appeared to influence the work reported in this paper.

Acknowledgement

This work was supported by the Natural Sciences and Engineering Research Council (NSERC) of Canada through a discovery grant to GW (RGPIN: 03140–2021). A portion of this work was performed at the National High Magnetic Field Laboratory (NHMFL), which is supported by the National Science Foundation Cooperative Agreement (DMR-2128556, DMR-1644779) and the State of Florida. The NMR user facility at the NHMFL is also supported by NIH P41GM122698 and RM1GM148766.

Data availability

Data will be made available on request.

References

[1] Y. Ba, J.A. Ripmeester, C.I. Ratcliffe, Water molecular reorientation in ice and tetrahydrofuran clathrate hydrate from lineshape analysis of ^{17}O spin-echo NMR spectra, Can. J. Chem. 89 (9) (2011) 1055–1064, https://doi.org/10.1139/v11-040.

[2] X. Kong, L.A. O'Dell, V. Terskikh, E. Ye, R. Wang, G. Wu, Variable-temperature ^{17}O NMR studies allow quantitative evaluation of molecular dynamics in organic solids, J. Am. Chem. Soc. 134 (35) (2012) 14609–14617, https://doi.org/10.1021/ja306227p.

[3] W.D. Wang, B.E.G. Lucier, V.V. Terskikh, W. Wang, Y. Huang, Wobbling and hopping: studying dynamics of CO_2 adsorbed in metal–organic frameworks via ^{17}O solid-state NMR, J. Phys. Chem. Lett. 5 (19) (2014) 3360–3365, https://doi.org/10.1021/jz501729d.

[4] M. Adjei-Acheamfour, R. Böhmer, Second-order quadrupole interaction based detection of ultra-slow motions: tensor operator framework for central-transition spectroscopy and the dynamics in hexagonal ice as an experimental example, J. Magn. Reson. 249 (2014) 141–149, https://doi.org/10.1016/j.jmr.2014.09.019.

[5] H.J. Jakobsen, H. Bildsøe, M. Brorson, Z. Gan, I. Hung, Quantitative dynamics and structure for crystalline Cs_2WO_4 and $KMnO_4$ determined from high-field ^{17}O variable-temperature MAS NMR experiments, J. Phys. Chem. C 118 (35) (2014) 20639–20646, https://doi.org/10.1021/jp505522a.

[6] M. Nava, N. Lopez, P. Müller, G. Wu, D.G. Nocera, C.C. Cummins, Anion-receptor mediated oxidation of carbon monoxide to carbonate by peroxide dianion, J. Am. Chem. Soc. 137 (46) (2015) 14562–14565, https://doi.org/10.1021/jacs.5b08495.

[7] M. Adjei-Acheamfour, M. Storek, J. Beerwerth, R. Böhmer, Two-dimensional second-order quadrupolar exchange powder spectra for nuclei with half-integer spins. Calculations and an experimental example using oxygen NMR, Solid State Nucl. Magn. Reson. 71 (2015) 96–107, https://doi.org/10.1016/j.ssnmr.2015.05.004.

[8] M. Adjei-Acheamfour, J.F. Tilly, J. Beerwerth, R. Böhmer, Water dynamics on ice and hydrate lattices studied by second-order central-line stimulated-echo oxygen-17 nuclear magnetic resonance, J. Chem. Phys. 143 (21) (2015) 214201, https://doi.org/10.1063/1.4936416. (Accessed 27 December 2024).

[9] G. Kim, J.M. Griffin, F. Blanc, S.M. Haile, C.P. Grey, Characterization of the dynamics in the protonic conductor CsH_2PO_4 by ^{17}O solid-state NMR spectroscopy and first-principles calculations: correlating phosphate and protonic motion, J. Am. Chem. Soc. 137 (11) (2015) 3867–3876, https://doi.org/10.1021/jacs.5b00280.

[10] Y. Dai, I. Hung, Z. Gan, G. Wu, Probing nitrite ion dynamics in $NaNO_2$ crystals by solid-state ^{17}O NMR, Concepts Magn. Reson. 45A (6) (2016), https://doi.org/10.1002/cmr.a.21409.

[11] E.G. Keeler, V.K. Michaelis, R.G. Griffin, ^{17}O NMR investigation of water structure and dynamics, J. Phys. Chem. B 120 (32) (2016) 7851–7858, https://doi.org/10.1021/acs.jpcb.6b05755.

[12] I. Hung, G. Wu, Z. Gan, Second-order quadrupolar line shapes under molecular dynamics: an additional transition in the extremely fast regime, Solid State Nucl. Magn. Reson. 84 (October 2016) (2017) 14–19, https://doi.org/10.1016/j.ssnmr.2016.11.002.

[13] J. Lu, I. Hung, A. Brinkmann, Z. Gan, X. Kong, G. Wu, Solid-state ^{17}O NMR reveals hydrogen-bonding energetics: not all low-barrier hydrogen bonds are strong, Angew. Chem. Int. Ed. 56 (2017) 6166–6170, https://doi.org/10.1002/anie.201700488.

[14] M. Adjei-Acheamfour, M. Storek, R. Böhmer, Communication: heterogeneous water dynamics on a clathrate hydrate lattice detected by multidimensional oxygen nuclear magnetic resonance, J. Chem. Phys. 146 (18) (2017) 181101, https://doi.org/10.1063/1.4983043, 2021/01/22.

[15] J. Beerwerth, M. Storek, D. Greim, J. Lueg, R. Siegel, B. Cetinkaya, W. Hiller, H. Zimmermann, J. Senker, R. Böhmer, Two-site jumps in dimethyl sulfone studied by one- and two-dimensional ^{17}O NMR spectroscopy, J. Magn. Reson. 288 (2018) 84–94, https://doi.org/10.1016/j.jmr.2018.01.016.

[16] Y. Dai, G. Wu, Solid-state ^{17}O NMR studies of sulfonate jump dynamics in crystalline sulfonic acids: insights into the hydrogen bonding effect, J. Phys. Chem. A 124 (46) (2020) 9597–9604.

[17] J. Beerwerth, B. Bojer, J. Senker, R. Böhmer, Time scales of the quasitetrahedral motion in $KMnO_4$ observed by ^{17}O central-transition NMR spectroscopy, J. Phys. Chem. C 124 (29) (2020) 16202–16208, https://doi.org/10.1021/acs.jpcc.0c04704.

[18] J. Beerwerth, R. Siegel, L. Hoffmann, L.S. Plaga, M. Storek, B. Bojer, J. Senker, W. Hiller, R. Böhmer, From ultraslow to extremely fast dynamics in sodium nitrate: an ^{17}O NMR study, Appl. Magn. Reson. 51 (7) (2020) 597–620, https://doi.org/10.1007/s00723-020-01201-5.

[19] C.-H. Chen, I. Goldberga, P. Gaveau, S. Mittelette, J. Špačková, C. Mullen, I. Petit, T.-X. Métro, B. Alonso, C. Gervais, et al., Looking into the dynamics of molecular crystals of ibuprofen and terephthalic acid using ^{17}O and ^{2}H nuclear magnetic resonance analyses, Magn. Reson. Chem. 59 (9–10) (2021) 975–990, https://doi.org/10.1002/mrc.5141, 2024/12/21.

[20] L. Hoffmann, J. Beerwerth, M. Adjei-Körner, V. Fuentes-Landete, C.M. Tonauer, T. Loerting, R. Böhmer, Oxygen NMR of high-density and low-density amorphous ice, J. Chem. Phys. 156 (8) (2022) 084503, https://doi.org/10.1063/5.0080333, 12/22/2024.

[21] I. Goldberga, N. Patris, C.-H. Chen, E. Thomassot, J. Trébosc, I. Hung, Z. Gan, D. Berthomieu, T.-X. Métro, C. Bonhomme, et al., First direct insight into the local environment and dynamics of water molecules in the whewellite mineral phase: mechanochemical isotopic enrichment and high-resolution ^{17}O and ^{2}H NMR analyses, J. Phys. Chem. C 126 (29) (2022) 12044–12059, https://doi.org/10.1021/acs.jpcc.2c02070.

[22] L. Vugmeyster, R. Fu, D. Ostrovsky, ^{17}O NMR relaxation measurements for investigation of molecular dynamics in static solids using sodium nitrate as a model compound, Solid State Nucl. Magn. Reson. 134 (2024) 101976, https://doi.org/10.1016/j.ssnmr.2024.101976.

[23] B.J. Rhodes, L.L. Schaaf, M.E. Zick, S.M. Pugh, J.S. Hilliard, S. Sharma, C.R. Wade, P.J. Milner, G. Csányi, A.C. Forse, ^{17}O NMR spectroscopy reveals CO_2 speciation and dynamics in hydroxide-based carbon capture materials, ChemPhysChem (2024) e202400941, https://doi.org/10.1002/cphc.202400941 n/a (n/a). (Accessed 29 December 2024).

[24] G. Wu, Solid-State ^{17}O NMR studies of organic and biological molecules: recent advances and future directions, Solid State Nucl. Magn. Reson. 73 (2016) 1–14, https://doi.org/10.1016/j.ssnmr.2015.11.001.

[25] R.P. Young, B.G. Caulkins, D. Borchardt, D.N. Bulloch, C.K. Larive, M.F. Dunn, L. J. Mueller, Solution-state ^{17}O quadrupole central-transition NMR spectroscopy in the active site of tryptophan synthase, Angew. Chem. Int. Ed. 55 (4) (2016) 1350–1354, https://doi.org/10.1002/anie.201508898, 2021/08/31.

[26] G. Wu, ^{17}O NMR studies of organic and biological molecules in aqueous solution and in the solid state, Prog. Nucl. Magn. Reson. Spectrosc. 114–115 (2019) 135–191, https://doi.org/10.1016/j.pnmrs.2019.06.002.

[27] J. Paulino, M. Yi, I. Hung, Z. Gan, X. Wang, E.Y. Chekmenev, H.-X. Zhou, T. A. Cross, Functional statbility of water wire-carbonyl interactions in an ion channel, Proc. Natl. Acad. Sci. USA. 117 (2020) 11908–11915.

[28] B. Lin, I. Hung, Z. Gan, P.H. Chien, H.L. Spencer, S.P. Smith, G. Wu, ^{17}O NMR studies of yeast ubiquitin in aqueous solution and in the solid state, Chembiochem 22 (5) (2021) 826–829.

[29] J. Shen, V. Terskikh, J. Struppe, A. Hassan, M. Monette, I. Hung, Z. Gan, A. Brinkmann, G. Wu, Solid-state ^{17}O NMR study of α-D-glucose: exploring new frontiers in isotopic labeling, sensitivity enhancement, and NMR crystallography, Chem. Sci. 13 (9) (2022) 2591–2603.

[30] J. Špačková, I. Goldberga, R. Yadav, G. Cazals, A. Lebrun, P. Verdié, T.-X. Métro, D. Laurencin, Fast and cost-efficient ^{17}O-isotopic labeling of carboxylic groups in biomolecules: from free amino acids to peptide chains, Chem. Eur J. 29 (10) (2023) e202203014, https://doi.org/10.1002/chem.202203014, 2024/12/29.

[31] R. Fu, A. Ramamoorthy, ^{17}O solid-state NMR spectroscopy of lipid membranes, J. Phys. Chem. B 128 (15) (2024) 3527–3537, https://doi.org/10.1021/acs.jpcb.4c01016.

[32] Z. Tian, E. Truong, W. Hu, J. Fan, R. Fu, T.A. Cross, X. Lin, R. Zhang, Y.-Y. Hu, Expanding the toolset of biomolecular NMR with efficient and cost-effective ^{17}O-labeling via bacterial expression, Chem. Eur J. (2024) e202403148, https://doi.org/10.1002/chem.202403148, 2024/12/08.

[33] I. Goldberga, I. Hung, V. Sarou-Kanian, C. Gervais, Z. Gan, J. Novák-Špačková, T.-X. Métro, C. Leroy, D. Berthomieu, A. van der Lee, et al., High-resolution ^{17}O solid-state NMR as a unique probe for investigating oxalate binding modes in materials: the case study of calcium oxalate biominerals, Inorg. Chem. 63 (22) (2024) 10179–10193, https://doi.org/10.1021/acs.inorgchem.4c00300.

[34] M. Witschas, H. Eckert, H. Freiheit, A. Putnis, G. Korus, M. Jansen, Anion rotation and cation diffusion in low-temperature sodium orthophosphate: results from solid-state NMR, J. Phys. Chem. A 105 (28) (2001) 6808–6816, https://doi.org/10.1021/jp003635t.

[35] N. Kim, C.P. Grey, Probing oxygen motion in disordered anionic conductors with ^{17}O and ^{51}V MAS NMR spectroscopy, Science 297 (5585) (2002) 1317–1320, https://doi.org/10.1126/science.1074130.

[36] M.R. Hampson, P. Hodgkinson, J.S.O. Evans, R.K. Harris, I.J. King, S. Allen, F. Fayon, The nature of oxygen exchange in ZrW_2O_8 revealed by two-dimensional solid-state ^{17}O NMR, Chem. Commun. (4) (2004) 392–393, https://doi.org/10.1039/B314076H, 10.1039/B314076H.

[37] L. Holmes, L. Peng, I. Heinmaa, L.A. O'Dell, M.E. Smith, R.-N. Vannier, C.P. Grey, Variable-temperature ^{17}O NMR study of oxygen motion in the anionic conductor $Bi_{26}Mo_{10}O_{69}$, Chem. Mater. 20 (2008) 3638–3648, https://doi.org/10.1002/chin.200835012.

[38] A. Soleihavoup, M.R. Hampson, S.J. Clark, J.S.O. Evans, P. Hodgkinson, Using ^{17}O solid-state NMR and first principles calculation to characterise structure and dynamics in inorganic framework materials, Magn. Reson. Chem. 45 (2007) S144–S155.

[39] M.H. Cohen, F. Reif, Quadrupole effects in nuclear magnetic resonance studies of solids, Solid State Phys. 5 (1957) 321–438.

[40] L. Frydman, J.S. Harwood, Isotropic spectra of half-integer quadrupolar spins from bidimensional magic-angle-spinning nmr, J. Am. Chem. Soc. 117 (19) (1995) 5367–5368.

[41] Z. Gan, I. Hung, X. Wang, J. Paulino, G. Wu, I.M. Litvak, P.L. Gor'kov, W.W. Brey, P. Lendi, J.L. Schiano, et al., NMR spectroscopy up to 35.2 T using a series-connected hybrid magnet, J. Magn. Reson. 284 (2017) 125–136, https://doi.org/10.1016/j.jmr.2017.08.007.

[42] G. Wu, D. Rovnyak, R.G. Griffin, Quantitative multiple-quantum magic-angle-spinning NMR spectroscopy of quadrupolar nuclei in solids, J. Am. Chem. Soc. 118 (39) (1996) 9326–9332.

[43] G. Wu, I. Hung, Z. Gan, V. Terskikh, X. Kong, Solid-state ^{17}O NMR study of carboxylic acid dimers: simultaneously accessing spectral properties of low- and high-energy tautomers, J. Phys. Chem. A 123 (38) (2019) 8243–8253, https://doi.org/10.1021/acs.jpca.9b07224.

[44] B.J. Rhodes, L.L. Schaaf, M.E. Zick, S.M. Pugh, J.S. Hilliard, S. Sharma, C.R. Wade, P.J. Milner, G. Csányi, A.C. Forse, ^{17}O NMR spectroscopy reveals CO_2 speciation and dynamics in hydroxide-based carbon capture materials, ChemPhysChem 26 (5) (2025) e202400941, https://doi.org/10.1002/cphc.202400941, 2025/03/25.

[45] H.J. Jakobsen, J. Skibsted, H. Bildsøe, N.C. Nielsen, Magic-angle spinning NMR spectra of satellite transitions for quadrupolar nuclei in solids, J. Magn. Reson. 85 (1) (1989) 173–180, https://doi.org/10.1016/0022-2364(89)90333-8.

[46] J. Skibsted, N.C. Nielsen, H. Bildsøe, H.J. Jakobsen, Satellite transitions in MAS NMR spectra of quadrupolar nuclei, J. Magn. Reson. 95 (1) (1991) 88–117, https://doi.org/10.1016/0022-2364(91)90327-P.

[47] G. Kunath, P. Losso, S. Steuernagel, H. Schneider, C. Jäger, ^{27}Al satellite transition spectroscopy (SATRAS) of polycrystalline aluminium borate $9Al_2O_3 \cdot 2B_2O_3$, Solid State Nucl. Magn. Reson. 1 (5) (1992) 261–266, https://doi.org/10.1016/0926-2040(92)90046-C.

[48] Z. Gan, Isotropic NMR spectra of half-integer quadrupolar nuclei using satellite transitions and magic-angle spinning, J. Am. Chem. Soc. 122 (2000) 3242–3243.

[49] S.E. Ashbrook, S. Wimperis, High-resolution NMR of quadrupolar nuclei in solids: the satellite-transition magic angle spinning (STMAS) experiment, Prog. Nucl. Magn. Reson. Spectrosc. 45 (1) (2004) 53–108, https://doi.org/10.1016/j.pnmrs.2004.04.002.

[50] M.J. Thrippleton, T.J. Ball, S. Steuernagel, S.E. Ashbrook, S. Wimperis, STARTMAS: a MAS-based method for acquiring isotropic NMR spectra of spin I=3/2 nuclei in real time, Chem. Phys. Lett. 431 (4) (2006) 390–396, https://doi.org/10.1016/j.cplett.2006.09.075.

[51] I. Hung, Z. Gan, High-resolution NMR of S = 3/2 quadrupole nuclei by detection of double-quantum satellite transitions via protons, J. Phys. Chem. Lett. 11 (12) (2020) 4734–4740, https://doi.org/10.1021/acs.jpclett.0c01236.

[52] T. Wolf, A. Eden-Kossoy, L. Frydman, Indirectly detected satellite-transition quadrupolar NMR via progressive saturation of the proton reservoir, Solid State Nucl. Magn. Reson. 125 (2023) 101862, https://doi.org/10.1016/j.ssnmr.2023.101862.

[53] S.E. Ashbrook, S. Antonijevic, A.J. Berry, S. Wimperis, Motional broadening: an important distinction between multiple-quantum and satellite-transition MAS NMR of quadrupolar nuclei, Chem. Phys. Lett. 364 (5) (2002) 634–642, https://doi.org/10.1016/S0009-2614(02)01412-4.

[54] S. Antonijevic, S.E. Ashbrook, S. Biedasek, R.I. Walton, S. Wimperis, H. Yang, Dynamics on the microsecond timescale in microporous aluminophosphate AlPO-14 as evidenced by ^{27}Al MQMAS and STMAS NMR spectroscopy, J. Am. Chem. Soc. 128 (24) (2006) 8054–8062, https://doi.org/10.1021/ja057682g.

[55] J.M. Griffin, S. Wimperis, A.J. Berry, C.J. Pickard, S.E. Ashbrook, Solid-state ^{17}O NMR spectroscopy of hydrous magnesium silicates: evidence for proton dynamics, J. Phys. Chem. C 113 (1) (2009) 465–471, https://doi.org/10.1021/jp808651x.

[56] M.T. Dunstan, J.M. Griffin, F. Blanc, M. Leskes, C.P. Grey, Ion dynamics in Li_2CO_3 studied by solid-state NMR and first-principles calculations, J. Phys. Chem. C 119 (43) (2015) 24255–24264, https://doi.org/10.1021/acs.jpcc.5b06647.

[57] P.J. Chu, B.C. Gerstein, Exchange dynamics of ^{23}Na and structural incommensuration in $NaMo_4O_6$: dynamic line shape for the second order central transition of quadrupolar nuclei, J. Chem. Phys. 90 (7) (1989) 3713–3727, https://doi.org/10.1063/1.455829, 12/27/2024.

[58] J.H. Kristensen, I. Farnan, Measurement of molecular motion in solids by nuclear magnetic resonance spectroscopy of half-integer quadrupole nuclei, J. Chem. Phys. 114 (21) (2001) 9608–9624, https://doi.org/10.1063/1.1368660, 12/22/2024.

[59] J.H. Kristensen, I. Farnan, Anisotropic relaxation and motion of half-integer quadrupole nuclei studied by central transition nuclear magnetic resonance spectroscopy, J. Magn. Reson. 158 (1) (2002) 99–125, https://doi.org/10.1016/S1090-7807(02)00065-4.

[60] R.W. Schurko, S. Wi, L. Frydman, Dynamic effects on the powder line shapes of half-integer quadrupolar nuclei: a solid-state NMR study of XO_4 groups, J. Phys. Chem. A 106 (1) (2002) 51–62, https://doi.org/10.1021/jp0130214.

[61] F.H. Larsen, Molecular dynamics of half-integer quadrupolar nuclei studied by QCPMG solid-state NMR experiments on static and rotating samples. Theory and simulations, J. Magn. Reson. 171 (2004) 293–304.

[62] R.L. Vold, G.L. Hoatson, Effects of jump dynamics on solid state nuclear magnetic resonance line shapes and spin relaxation times, J. Magn. Reson. 198 (1) (2009) 57–72, https://doi.org/10.1016/j.jmr.2009.01.008.

[63] A. Abragam, The Principles of Nuclear Magnetism, Oxford University Press, 1961.

[64] J.A. Pople, The effect of quadrupole relaxation on nuclear magnetic resonance multiplets, Mol. Phys. 1 (1958) 168–174.

[65] L. Werbelow, NMR linewidths of spin-1/2 nuclei coupled to higher order spins, J. Magn. Reson. 67 (1986) 66–72.

[66] R.L. Mieher, Nuclear relaxation via quadrupole coupling, Phys. Rev. Lett. 4 (1960) 57–59.

[67] Y. Dai, ^{17}O NMR Spectrosopic Studies of Molecular Dynamics in Solids, Queen's University, Kingston, Ontario, Canada, 2021. Ph. D. Thesis.

[68] D. Jardón-Álvarez, M.O. Bovee, J.H. Baltisberger, P.J. Grandinetti, Natural abundance ^{17}O and ^{33}S nuclear magnetic resonance spectroscopy in solids achieved through extended coherence lifetimes, Phys. Rev. B 100 (14) (2019) 140103, https://doi.org/10.1103/PhysRevB.100.140103.

[69] I. Majerz, M.J. Gutmann, Mechanism of proton transfer in the strong OHN intermolecular hydrogen bond, RSC Adv. 1 (2011) 219–228.

[70] I. Majerz, M.J. Gutmann, Temperature-dependent signle-crystal neutron diffraction study of the strong OHN hydrogen bond in pyridinium 2,4-dinitrobenzoate, J. Phys. Chem. A 112 (2008) 9801–9806.